Defense Threat Reduction Agency
8725 John J. Kingman Road, MS
6201 Fort Belvoir, VA 22060-6201

DTRA-TR-22-142

TECHNICAL REPORT

Spin Based Low Field Magnetoresistance as a Novel Tool for the Investigation of Radiation Effects in 3D and Vertically Integrated Microstructures

September 2022

HDTRA1-18-1-0012

Prepared by:
Michael E. Flatte

University of Iowa,
Iowa City, IA
52242-1479

REPORT DOCUMENTATION PAGE

1. REPORT DATE	2. REPORT TYPE	3. DATES COVERED	
		START DATE	END DATE
November 1, 2022	Final	03/07/2018	03/06/2022

4. TITLE AND SUBTITLE
Spin Based Low Field Magnetoresistance as a Novel Tool for the Investigation of Radiation Effects in 3D and Vertically Integrated Microstructures

5a. CONTRACT NUMBER	5b. GRANT NUMBER	5c. PROGRAM ELEMENT NUMBER
	HDTRA1-18-1-0012	
5d. PROJECT NUMBER	**5e. TASK NUMBER**	**5f. WORK UNIT NUMBER**

6. AUTHOR(S)
Michael E. Flatté and Patrick M. Lenahan

7. PERFORMING ORGANIZATION NAME(S) AND ADDRESS(ES)
University of Iowa, Iowa City, IA 52242
Pennsylvania State University, State College, PA 16801

8. PERFORMING ORGANIZATION REPORT NUMBER
N/A

9. SPONSORING/MONITORING AGENCY NAME(S) AND ADDRESS(ES)	10. SPONSOR/MONITOR'S ACRONYM(S)	11. SPONSOR/MONITOR'S REPORT NUMBER(S)
Defense Threat Reduction Agency/AL-ACR 8725 John J. Kingman Rd. Ft. Belvoir, VA 22060-6201	DTRA	DTRA-TR-22-142

12. DISTRIBUTION/AVAILABILITY STATEMENT
Distribution Statement A - Approved for public release; distribution is unlimited

13. SUPPLEMENTARY NOTES

14. ABSTRACT
We have extensively explored the near zero field magnetoresistance (NZFMR) effects, due to spin-dependent recombination (SDR), spin-dependent charge pumping (SDCP) and spin-dependent trap-assisted tunneling (SDTAT) in devices (principally MOSFETs) that have been irradiated or have undergone electrical stress to mimic the effects of radiation. We have correlated the amount of stress to the defect density and effects on NZFMR. In addition to Si MOSFETs we have conducted studies of amorphous hydrogenated silicon and silicon nitride films, aluminum oxide gate oxides, and SiC MOSFETs. We have been able to correlate amount of damage with NZFMR. We have been able to identify defect dynamics (trapping/detrapping rates) in the curves directly. Finally we have demonstrated that we can observe NZFMR features in commercially packaged CMOS devices, in which the electrically-detected magnetic resonance (EDMR) features are invisible. This validates the central idea of this project; we conclude that NZFMR is an effective method of identifying radiation damage in 3D and vertically integrated devices in which the EDMR features are not visible due to the presence of nearby conducting layers that screen the microwaves.

15. SUBJECT TERMS
Magnetoresistance, Radiation Effects, Microstructures, integrated circuits, IC, near zero field magnetoresistance, NZFMR, spin-dependent recombination, SDR, spin-dependent charge pumping, SDCP, spin-dependent trap-assisted tunneling, SDTAT, MOSFETs, Testing

16. SECURITY CLASSIFICATION OF:

a. REPORT	b. ABSTRACT	C. THIS PAGE	17. LIMITATION OF ABSTRACT	18. NUMBER OF PAGES
U	U	U	SAR	26

19a. NAME OF RESPONSIBLE PERSON	19b. PHONE NUMBER *(Include area code)*
Jacob Calkins, DTRA	571-616-5946

INSTRUCTIONS FOR COMPLETING SF 298

1. REPORT DATE.
Full publication date, including day, month, if available. Must cite at least the year and be Year 2000 compliant, e.g. 30-06-1998; xx-06-1998; xx-xx-1998.

2. REPORT TYPE.
State the type of report, such as final, technical, interim, memorandum, master's thesis, progress, quarterly, research, special, group study, etc.

3. DATES COVERED.
Indicate the time during which the work was performed and the report was written.

4. TITLE.
Enter title and subtitle with volume number and part number, if applicable. On classified documents, enter the title classification in parentheses.

5a. CONTRACT NUMBER.
Enter all contract numbers as they appear in the report, e.g. F33615-86-C-5169.

5b. GRANT NUMBER.
Enter all grant numbers as they appear in the report, e.g. AFOSR-82-1234.

5c. PROGRAM ELEMENT NUMBER.
Enter all program element numbers as they appear in the report, e.g. 61101A.

5d. PROJECT NUMBER.
Enter all project numbers as they appear in the report, e.g. 1F665702D1257; ILIR.

5e. TASK NUMBER. Enter all task numbers as they appear in the report, e.g. 05; RF0330201; T4112.

5f. WORK UNIT NUMBER.
Enter all work unit numbers as they appear in the report, e.g. 001; AFAPL30480105.

6. AUTHOR(S). Enter name(s) of person(s) responsible for writing the report, performing the research, or credited with the content of the report. The form of entry is the last name, first name, middle initial, and additional qualifiers separated by commas, e.g. Smith, Richard, J, Jr.

7. PERFORMING ORGANIZATION NAME(S) AND ADDRESS(ES). Self-explanatory.

8. PERFORMING ORGANIZATION REPORT NUMBER.
Enter all unique alphanumeric report numbers assigned by the performing organization, e.g. BRL-1234; AFWL-TR-85-4017-Vol-21-PT-2.

9. SPONSORING/MONITORING AGENCY NAME(S) AND ADDRESS(ES). Enter the name and address of the organization(s) financially responsible for and monitoring the work.

10. SPONSOR/MONITOR'S ACRONYM(S). Enter, if available, e.g. BRL, ARDEC, NADC.

11. SPONSOR/MONITOR'S REPORT NUMBER(S). Enter report number as assigned by the sponsoring/monitoring agency, if available, e.g. BRL-TR-829; -215.

12. DISTRIBUTION/AVAILABILITY STATEMENT. Use agency-mandated availability statements to indicate the public availability or distribution limitations of the report. If additional limitations/ restrictions or special markings are indicated, follow agency authorization procedures, e.g. RD/ FRD, PROPIN, ITAR, etc. Include copyright information.

13. SUPPLEMENTARY NOTES. Enter information not included elsewhere such as: prepared in cooperation with; translation of; report supersedes; old edition number, etc.

14. ABSTRACT. A brief (approximately 200 words) factual summary of the most significant information.

15. SUBJECT TERMS. Key words or phrases identifying major concepts in the report.

16. SECURITY CLASSIFICATION. Enter security classification in accordance with security classification regulations, e.g. U, C, S, etc. If this form contains classified information, stamp classification level on the top and bottom of this page.

17. LIMITATION OF ABSTRACT. This block must be completed to assign a distribution limitation to the abstract. Enter UU (Unclassified Unlimited) or SAR (Same as Report). An entry in this block is necessary if the abstract is to be limited.

FINAL REPORT

Grant/Award #: HDTRA1-18-1-0012

PI Name: Michael E. Flatté

Organization/Institution: University of Iowa

Co-PI Name: Patrik M. Lenahan

Organization/Institution: Pennsylvania State University

Project Title: Spin Based Low Field Magnetoresistance as a Novel Tool for the Investigation of Radiation Effects in 3D and Vertically Integrated Microstructures

Major goals of the project

This project was an interdisciplinary, multi-university study which developed a new approach to study total dose radiation effects in electronic devices within fully processed three-dimensional and vertically integrated circuits. Our approach was to develop and apply a newly discovered technique of making very sensitive measurements of defect-induced electronic transport within functioning device structures at room temperature. The very sensitive measurements of defects are made by measuring the changed electrical current in small (<1000 Gauss) magnetic fields. Although these small magnetic fields do not affect high-conductivity regions much, they substantially perturb the spin correlations between defects, which alters the electrical transport through lower-conducting regions, including tunnel barriers, depletion regions, silicon/dielectric interface regions and dielectric films used in memory devices. This approach provided fundamental atomic scale understanding of some aspects of radiation damage in fully processed 3D and vertically integrated devices. The major goals were:

Task 1: (U. Iowa): Develop theory and modeling of radiation-induced defect energies on low-field magnetoresistance in static magnetic fields due to spin correlations. Conductivity will be calculated using the stochastic Liouville equation for correlated spin centers including hyperfine interactions and inhomogeneous Landé g tensors. Theory and modeling will be performed for a variety of devices within 3D and vertically integrated microstructures before and after irradiation, according to the systems experimentally measured at Penn State in Task 2.

Task 2: (Penn State): Develop measurement techniques to explore charge magneto-transport involving radiation-induced defects in 3D and vertically integrated microstructures. Carry out such measurements on a variety of devices within 3D and vertically integrated microstructures before irradiation and after irradiation at various levels under technologically meaningful conditions. This study shall involve the exploration of technologically meaningful differences in materials chemistry to the greatest possible extent. These results will be compared with the theoretical developments at U. Iowa provided in Task 1.

Accomplishments

We have extensively explored the near zero field magnetoresistance (NZFMR) effects, due to spin-dependent recombination (SDR), spin-dependent charge pumping (SDCP) and spin-dependent trap-assisted tunneling (SDTAT) in devices (principally MOSFETs) that have been irradiated or have undergone electrical stress to mimic the effects of radiation. We have correlated the amount of stress to the defect density and effects on NZFMR. In addition to Si MOSFETs we have conducted studies of amorphous hydrogenated silicon and silicon nitride films, aluminum oxide gate oxides, and SiC MOSFETs. We have been able to correlate amount of damage with NZFMR. We have been able to identify defect dynamics (trapping/detrapping rates) in the curves directly. Finally we have demonstrated that we can observe NZFMR features in commercially packaged CMOS devices, in which the electrically-detected magnetic resonance (EDMR) features are invisible. This validates the central idea of this project; we conclude that NZFMR is an effective method of identifying radiation damage in 3D and vertically integrated devices in which the EDMR features are not visible due to the presence of nearby conducting layers that screen the microwaves. A detailed discussion of these results follows.

NZFMR of Radiation induced Interface Traps in Si MOSFETs

We compared low field EDMR and SDR /NZFMR observations of radiation induced P_b center interface traps to theoretical predictions of the NZFMR response expected based on a stochastic Liouville equation approach using reasonable values for the hyperfine interactions which would be involved in Pb center recombination processes. We achieved a remarkably close agreement between experiment and theory as illustrated [4] in Figure 1.

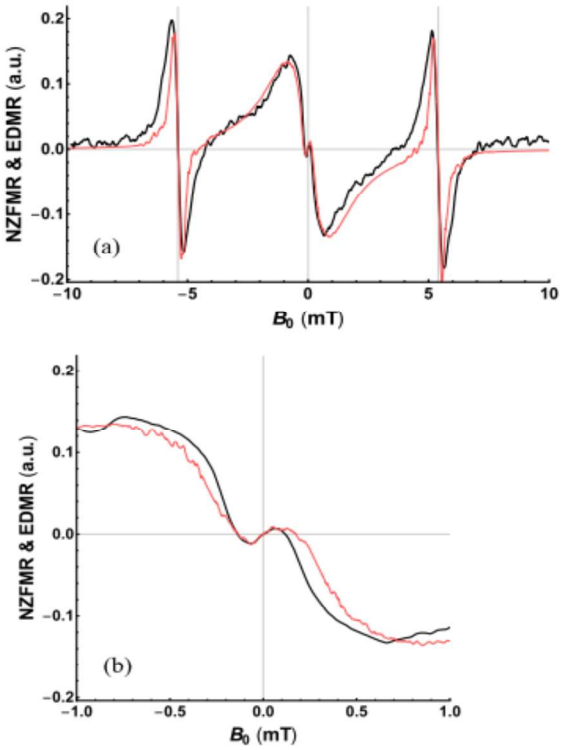

Figure 1. Post irradiation NZFMR traces [4]. The black traces are experimentally determined and the red traces are calculated based on reasonable estimates of hyperfine interactions. The upper panel traces are over +10 to-10 mT whereas the lower panel traces are over -1 to +1 mT. Note the close correspondence between the experimental and theoretical results.

B. **NZFMR of Radiation Induced Gate Oxide Traps**

We compared SDTAT/NZFMR and SDTAT/EDMR traces on radiation induced leakage currents in gate oxides, and to simulations. We compared the SDTAT EDMR traces to simulations of the EPR spectra expected from a superposition of oxide interface Pb defects and oxide E' centers. The signal to noise ratios in these measurements were modest but they suggest that radiation induced leakage currents involve an interaction between interface and oxide centers. A role for interface defects in oxide leakage (caused not by radiation but by electrical stressing) has been proposed by Nicollian some time ago. (P. E. Nicollian et al. Proceedings of the 37th Annual IEEE International Reliability Physics Symposium, March 1999, pp.400-404) This study strongly suggests that the radiation induced leakage currents also, surprisingly, involve interface traps but also oxide silicon dangling bond defects known as E' centers. Representative results are shown in Figure 2 (e.g. [3]). Although the study included both EDMR and NZFMR data, in this case the relatively low signal to noise NZFMR as yet precludes direct defect identification.

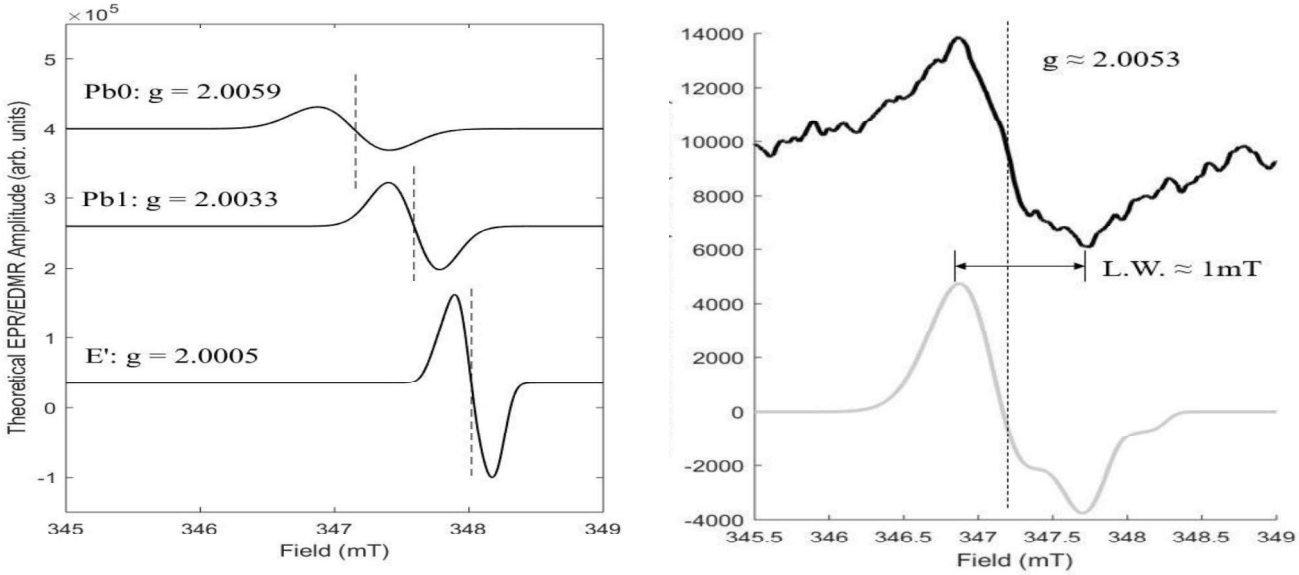

Figure 2. Left: Simulated EPR traces for each of the three defects involved. A modulation amplitude of 0.32 mT, and equal populations of each defect are assumed. Right: EDMR trace with the magnetic field oriented parallel to the (100) interface normal (top) and weighted addition of the three curves shown in the left of the figure 2 (bottom) (Figure adapted from Ref. 3).

C. Validating NZFMR as a Spectroscopic Technique With Analytical Power for MOSFETs

Substantial progress has beeen made in two parallel studies in which more advanced applications of the stochastic Liouvile equation have been utilized. We have been able to derive spectra which almost exactly match the NZFMR and low field EDMR responses, that is, the NZFMR and EDMR spectra over a range of source/ drain to body junction voltages. These voltage changes yield significant changes in line shape. We utilized reasonable estimates of hyperfine parameters involving nearby magnetic silicon and hydrogen nuclei in these calculations. These voltages represent a significant range in silicon/ silicon dioxide interrface quasi-Fermi energies and thus interface region charge carrier densities. Representative results [14] are shown in Figure 3.

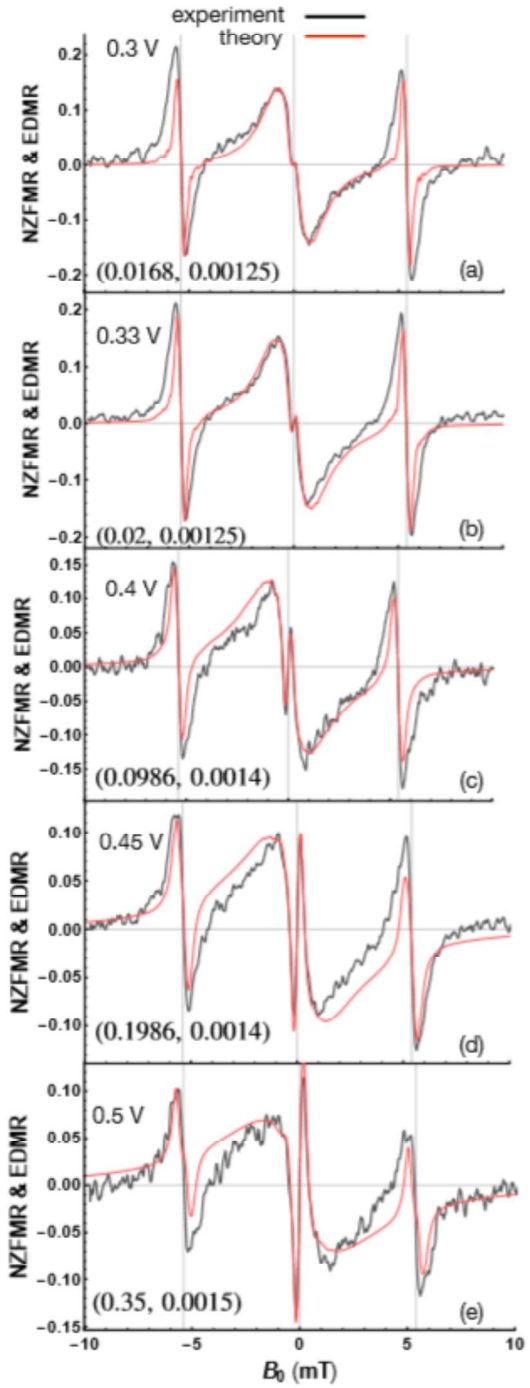

Figure 3: Experimental and model NZFMR and EDMR line shapes [14]. Experimental curves have been scaled by a constant factor to fit with the model. Each panel displays the values of (k_S, k_D) used in the model in order to show qualitative comparisons. Hyperfine interactions are in order to show qualitative comparisons. Hyperfine interactions are a_e = 0.15 mT and a_{Pb} = 0.5 mT. Other parameters are g = 2, B_1 =0.02 mT, f = 150 MHz (5.4 mT). The model curve in each panel averaged 20000 different nuclear field configurations.

We simultaneously pursued a different approach, which however is also based upon the stochastic Liouville equation, to analyze NZFMR measurements. In two systems, one of which involves NZFMR observed in trap assisted tunneling current and a second case, spin dependent recombination NZFMR. We obtained reasonable agreement with theory and experiment in both systems. We can extract hyperfine parameters utilizing a multi-variable least squares fitting of experimental NZFMR results and models based on the stochastic quantum Liouville equation. We

analyzed SDTAT/NZFMR results in amorphous hydrogenated silicon thin films and SDR/NZFMR in silicon/ silicon dioxide MOSFETs which had been subjected to gamma irradiation. In both cases, the hyperfine interactions, were taken to be from magnetic silicon and hydrogen nuclei. Representative results are shown in Figure 4 for radiation induced P_b center interface trap SDR/ NZFMR [6] and Figure 5 for SDTAT/ NZFMR of silicon dangling bonds [6] in an amorphous hydrogenated silicon thin film.

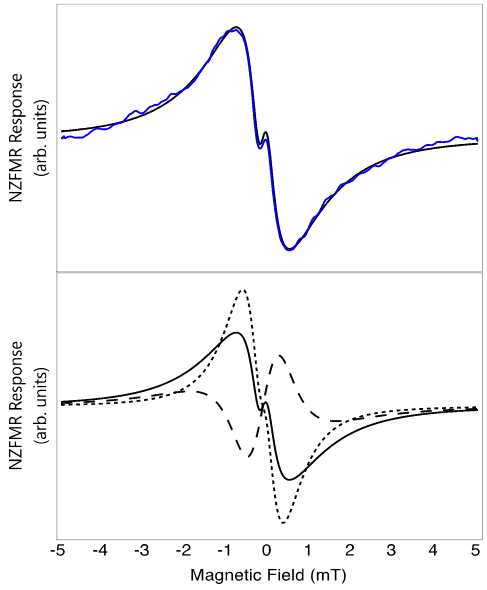

Figure 4. Analysis of NZFMR results on an irradiated MOSFET [6]. Upper figure compares a fitted spectrum in black with a blue experimentally determined spectrum; the fitted spectrum is a superposition of contributions (lower figure) from Pb center hyperfine interactions with magnetic silicon nuclei (long dash) and nearby hydrogen nuclei (short dash).

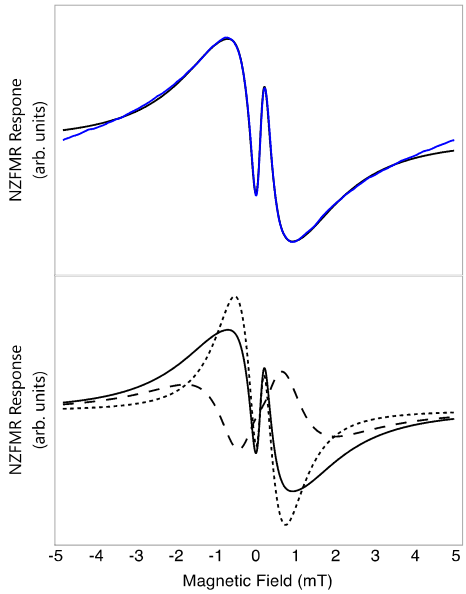

Figure 5: [6] Upper Figure: a-Si:H SDTAT NZFMR experimental spectrum (blue). Fitted NZFMR spectrum (solid black) that is the superposition of the contributions due to hopping from site A to site A (short dash) and hopping from site A to Site B (long dash).

D. Exploration of Defect Trapping Kinetics in the Silicon-Silicon Dioxide System

In addition to providing information about defect structure, the stochastic Liouville approach should also be able to provide information about charge capture and emission by varying the time involved in measurements. We observed these effects in the silicon/ silicon dioxide MOS system using NZFMR spin dependent charge pumping. These results are summarized in figure 6, which shows NZFMR spin dependent charge pumping (SDCP). The NZFMR/SDCP spectrum clearly

depends upon the frequency and shape (sinusoidal or trapezoidal) of the wave form utilized. From many other measurements, we know that the defects detected are interface dangling bonds, P_b centers. Although the signal to noise ratio in these measurements is mediocre, the results clearly show that the linewidth depends upon the details of the measurement. (Since the amplitude of the NZFMR/SDCP wave form is the same in all cases, the defects detected are the same in each case.)

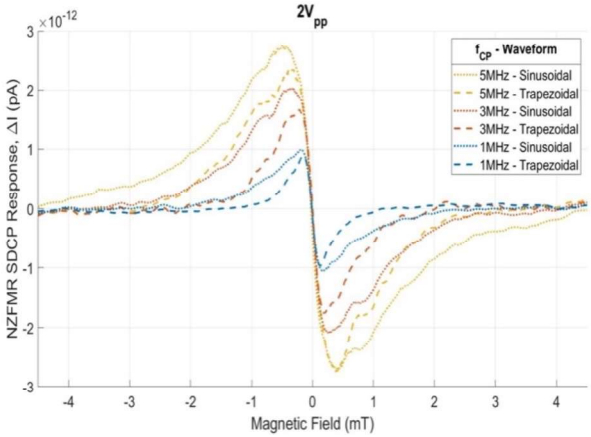

Figure 6: Plots of NZFMR SDCP taken at various frequencies utilizing sinusoidal and trapezoidal wave forms.

These "proof of concept" measurements indicate strongly that an analysis of NZFMR results using the stochastic Liouville equation approach provides insight into the kinetics of charge capture and emission from defects of great technological importance.

E. Direct Relationship Between NZFMR Response and Defect Density

A question of particular interest in our development of NZFMR as an analytical tool is whether or not we can relate the NZFMR amplitude to a paramagnetic defect density. We have begun to investigate this question and have some encouraging results obtained on high electric field stressed MOS devices. The devices utilized have been provided by Sandia National Laboratories.

The oxide thickness of the Si/SiO_2 MOSFETs is 7.5 nm and the gate stressing voltage was -9 V. Although the stressing utilized in the measurements is due to high oxide electric fields, we know that the high field stressing induced defects at the Si/SiO_2 interface are similar to those generated by ionizing radiation. As shown by Fitzgerald and Grove [Surface Science **9**, 347 (1968)], the recombination current peak in an appropriately configured and biased MOSFET is proportional to the interface trap density, with a constant of proportionality which can be determined from readily available parameters. We have measured these peaks and also measured the NZFMR amplitude (determined from zero field induced changes in the peak) at three different stressing times which yield significantly different amplitudes. Results of the electrical measurements of the recombination current are shown in Fig. 7. Results of the

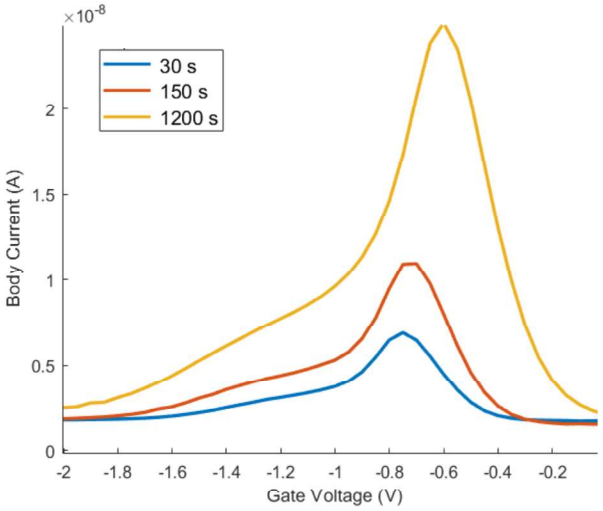

Fig. 7: DCIV electrical measurements for 7.5 nm Si/SiO_2 MOSFETs after -9 V constant gate stressing for 30 seconds, 150 seconds, and 1200 seconds.

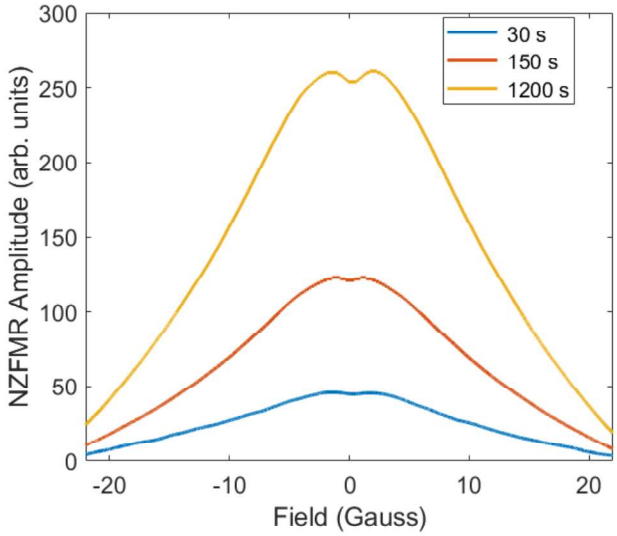

Fig. 8: NZFMR DCIV 7.5 nm Si/SiO_2 MOSFETs after -9 V constant gate stressing for 30 seconds, 150 seconds, and 1200 seconds.

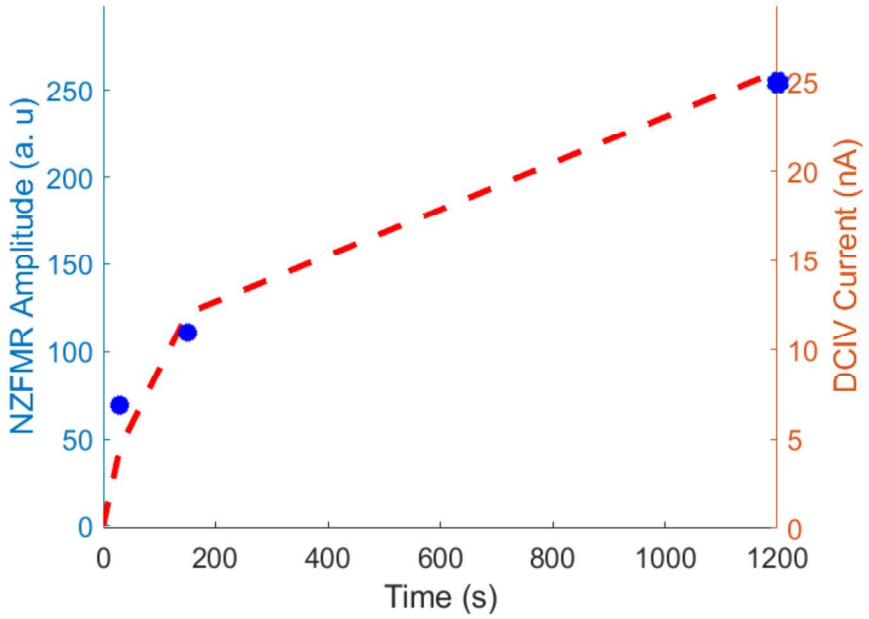

Fig. 9: NZFMR amplitudes (blue) vs. stress time and DCIV recombination current (red) vs. stress time.

NZFMR response are shown in Fig. 8 and a plot of NZFMR amplitude versus recombination current amplitude are shown in Fig. 9.

Within experimental error, the NZFMR and the recombination current peak amplitudes are proportional to one another. Although these results are limited to just a few data points and a single system, they strongly indicate that the NZFMR response is proportional to the relevant defect densities. The constant of proportionality can be determined, at least in this case, to fairly high precision. These results should be viewed as preliminary but with the understanding that the devices and defects involved in these measurements are quite important in radiation hard electronics.

Correlation of time dependent dielectric breakdown and NZFMR linewidth for Si MOSFETs

Electrically detected magnetic resonance and near-zero-field magnetoresistance measurements were used to study atomic-scale traps generated during high-field gate stressing in Si/SiO_2 MOSFETs. The defects observed are almost certainly important to time-dependent dielectric breakdown. The measurements were made with spin-dependent recombination current involving defects at and near the Si/SiO_2 boundary. The interface traps observed are P_{b0} and P_{b1} centers, which are silicon dangling bond defects. The ratio of P_{b0}/P_{b1} is dependent on the gate stressing polarity. Electrically detected magnetic resonance measurements also reveal generation of E^0 oxide defects near the Si/SiO_2 interface. Near-zero-field magnetoresistance measurements made throughout stressing reveal that the local hyperfine environment of the interface traps changes with stressing time; these changes are almost certainly due to the redistribution of hydrogen near the interface.

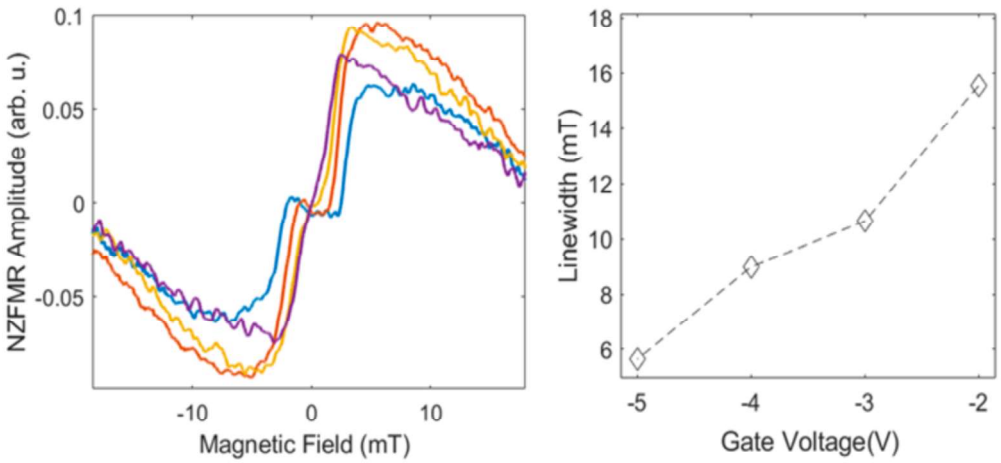

Fig. 10 Comparisons of NZFMR SDTAT in Si/SiO_2 MOSFETs stressed at – 9 V for 60 minutes at various gate biases. The significant change in linewidths (5-16 mT) is due in part from band-bending in the MOS kinetics of the trap- assisted tunneling process [11].

We were able to study time-dependent dielectric breakdown (TDDB) with NZFMR in Si/SiO_2 transistors. This involved an analysis of the effect that gate bias had on the spin-dependent

trap-assisted tunneling (SDTAT) spectrum of a highly stressed MOS array, showing large changes in linewidths in the tunneling processes as shown in Fig. 10 (Ref. 11).

F. Silicon- Silicon Dioxide NZFMR/EDMR Studies to explore H-complexed E' and related centers (^{29}Si-Depleted and Unpassivated Si/SiO_2)

We have investigated a comparison study of the NZFMR response of four sets of otherwise identical Si/SiO2 structures, each with very different populations of magnetic nuclei. The NZFMR response was detected through spin dependent trap assisted tunneling through the oxides. In one set of samples, the silicon is quite highly depleted of ^{29}Si and the oxides were not subjected to a forming gas anneal (5% H_2 and 95% N_2). Hydrogen nuclei all possess magnetic nuclei, nearly all of the have a nuclear spin of ½. The ^{29}Si nuclei also have a spin of ½, whereas the remaining silicon isotopes ^{28}Si are nonmagnetic. In a second set of structures, the silicon is depleted of the magnetic ^{29}Si isotope silicon, but the oxides were subjected to the H_2 containing forming gas anneal. In a third set of samples, the structures have the naturally abundant 4.7% ^{29}Si nuclei but were not subjected to the forming gas. In a fourth set of samples both the ^{29}Si and the H_2, due to the forming gas, is present. In figure 11, we illustrate the dramatic differences in the near zero field spectra of the four samples. In each of the traces, all device dimensions and spectrometer setting are, within experimental error, identical. Note that the traces are integrals of the "raw" NZFMR data. Due to the lock in detection technique, the "raw" data appears as an approximate derivative of the NZFMR current change versus magnetic field.

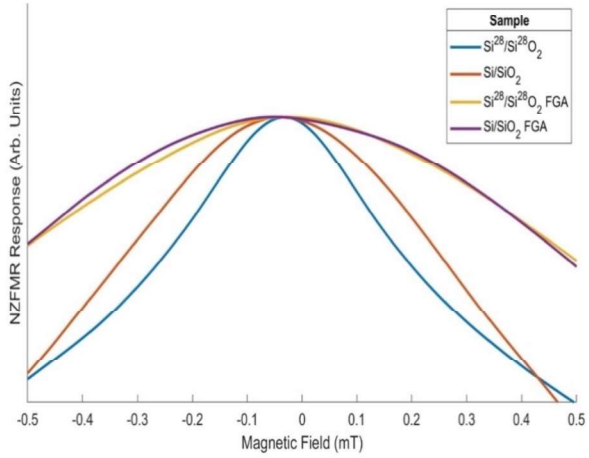

Figure 11: Representative NZFMR traces from four sets of Si/SiO_2 structures with very different concentrations of magnetic nuclei. Adapted from Ref. 9.

The results of figure 11, clearly, though only qualitatively, illustrate the effects of hyperfine interactions on the NZFMR response. Of particular interest is the case of the non-hydrogen passivated structures depleted of ^{29}Si. In these structures, there are essentially no magnetic nuclei present, thus, for those samples, we would expect that the NZFMR and EDMR (at very low magnetic fields) would solely involve dipolar interactions. In figure 12, we illustrate a very low field EDMR spectrum taken on the non-hydrogen passivated ^{29}Si depleted structures [10]. The insert at the upper left in the figure was taken at half the resonance field.

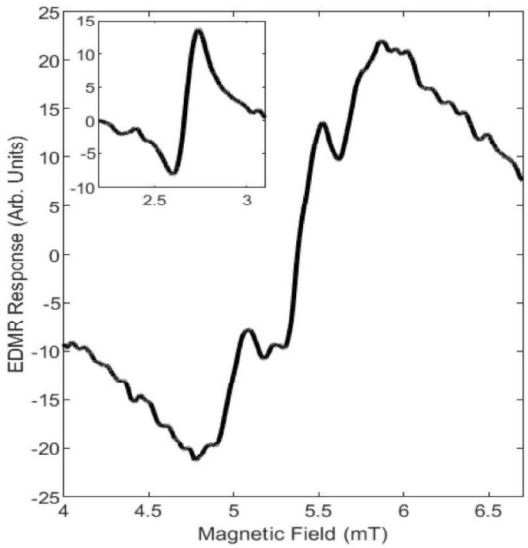

Figure 12: This figure illustrates a very low magnetic field EDMR trace taken on the unpassivated ^{29}Si depleted sample. The insert in the upper left of the figure is the response at half the resonance field [10].

In figure 13, we illustrate the integrals corresponding to the lock-in detected EDMR traces of figure 12, with the half-field integrated response appearing on the lower right inset in this case[10].

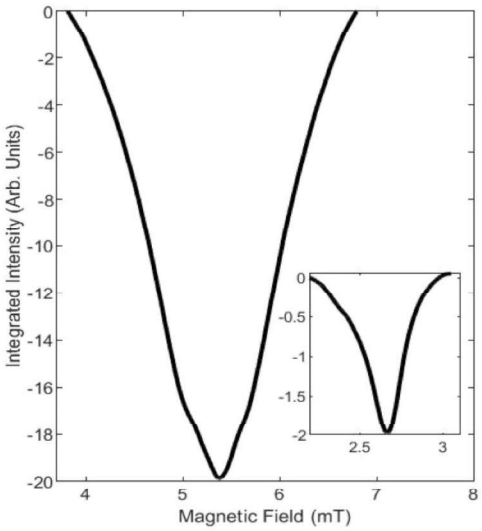

Figure 13: This figure [10] illustrates integrals of the low field and half field EDMR traces shown in figure 2. Recall, the sample in this case is unpassivated and is also depleted of ^{29}Si.

Due to the absence of hyperfine interactions, a very weak half field response becomes visible. The half field response is due to the dipolar coupling between nearby paramagnetic defects. It is possible to determine the distance between the spins utilizing an approach which was first pointed out by Slichter (*Principles of Magnetic Resonance*, Springer-Verlag, Berlin, 1978) extended to EPR by Eaton et al. [JACS 105, 6560 (1983)] and adapted to EDMR by Cochrane et al. [APL 104, 093503 (2014)]. Using this approach, one may calculate) at least to first order) the magnitude of the dipole-dipole interactions. The half field measurements indicate a dipole field contribution of about 0.3 mT.

In figure 14, we illustrate a wide magnetic field scan from -10 to +10 mT which shows both the full and half field EDMR spectra and the NZFMR response [10]. The signal to noise ratio in this scan is fairly modest due to the inherent trade offs in scan with, signal average time and lock-in time constant as well as the requirement that the magnetic field modulation amplitude had to be set at a very low value to allow observation of all three varieties of response. Note that the NZFMR phase and the half field and full field phases are inverted.

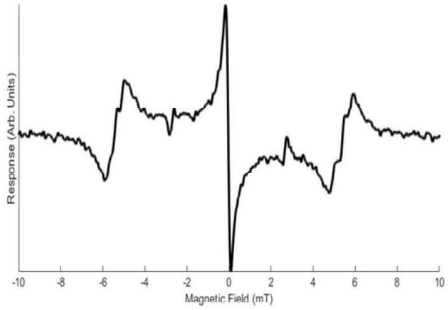

Figure 14. A representative plot of the NZFMR half field and full field EDMR response in the non-passivated ^{29}Si depleted devices. Ref. 10.

We have utilized the stochastic Liouville formalism to model the anticipated EDMR response. From this model it is possible to independently measure the dipolar contribution. As discussed below, the overall correspondence between the stochastic Liouville based simulation and experiment and the non-passivated ^{29}Si depleted devices is excellent. The dipolar contribution extracted from the calculations is within about 5% of the value obtained in the half field measurement; the close agreement should probably be viewed as fortuitously good.

The experimental results of the non-passivated, ^{29}Si depleted MIS capacitors suggest the EDMR and NZFMR signals may be due to abundance of dangling bond defects at the Si/SiO_2 interface via dipolar interactions. For the first time, EDMR with solely dipolar (no hyperfine) interactions were modeled using the stochastic Liouville formalism in the following manner: one spin is considered to be at a defect (possibly an E' within the oxide layer, one spin at a dangling bond at the interface; the current path is between these two defects. A third spin lies on the interfacial plane along a direction perpendicular to the current path (making an angle θ=0 in dipolar Hamiltonian). It is these two latter spins that interact via dipolar coupling. The EDMR produced from the calculation is shown in Fig. 15. The right panel of Fig. 15 should be compared to experimental trace of Fig. 12 and the left panel of Fig. 15 should be compared to the experimental traces of Fig. 13. Fig. 15 is adapted from Ref. 10.

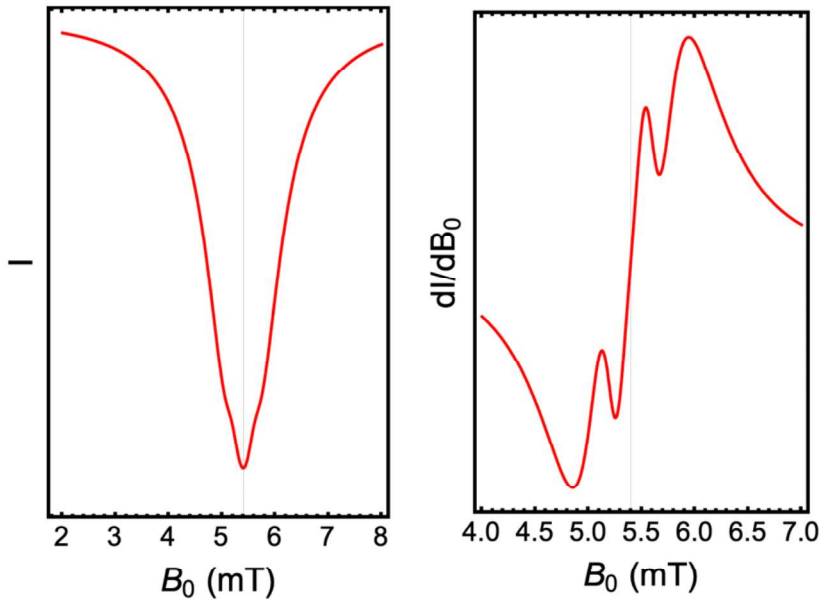

Figure 15. Left: Modeled EDMR trace (corresponds to integrated experimental trace). Right: derivative of left panel. Note the close correspondence between the theoretical results of these figures and the experimental results of figures 2 and 3. Adapted from Ref. 10.

The calculations assumed $\mathrm{d} \ll B_0$ which permits a simplification of the dipolar Hamiltonian used (and for rotating wave approximation to be valid). The emergence of the finer EDMR features with the elimination of nearly all nuclear moment sources and the qualitative agreement between model and experiment point to the pivotal role that dipolar interactions may play in governing EDMR line shapes. From the model, we obtained a dipolar field of $B_{dip} = \frac{d}{g\,\mu_B} \approx 0.3\ mT$.

A half-field resonance, induced by the dipolar interaction, and observed in the experimental traces of Fig. 14 is also calculated from the model – see Fig. 16

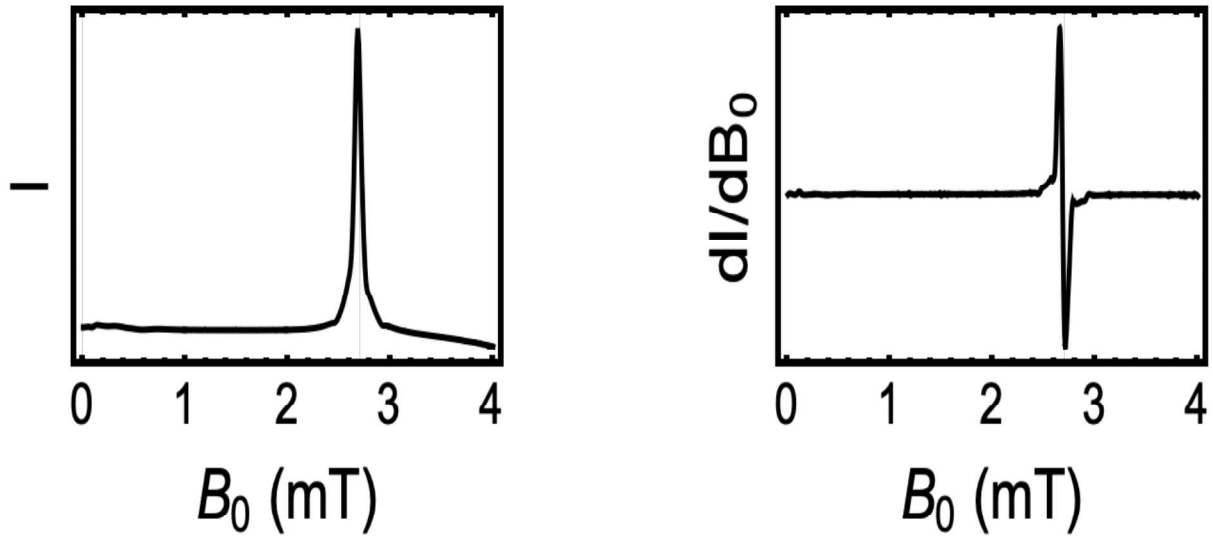

Figure 16. Left: Modeled EDMR trace showing the dipolar induced half-field resonance (full field resonance is near 5.4 mT and not shown). Right: derivative of left panel.

The role of the dipolar interaction for NZFMR was discovered to be subtle. The secular terms do not give rise to a magneto-effect due to the similarity of gyromagnetic ratios of the three pertinent spins. This is understood by transforming the stochastic Liouville equation to a so-called rotating reference frame where the applied field (so Zeeman term) is zero. When doing so the dipolar Hamiltonian is unchanged. However, the same does not occur when treating the non-secular terms (which are often ignored in EPR). We find that it is the non-secular portion of the dipolar coupling that does give rise to a NZFMR effect. These same terms make negligible contributions to the full field EDMR resonances. The results from NZFMR and the full-field EDMR are shown in Fig. 17.

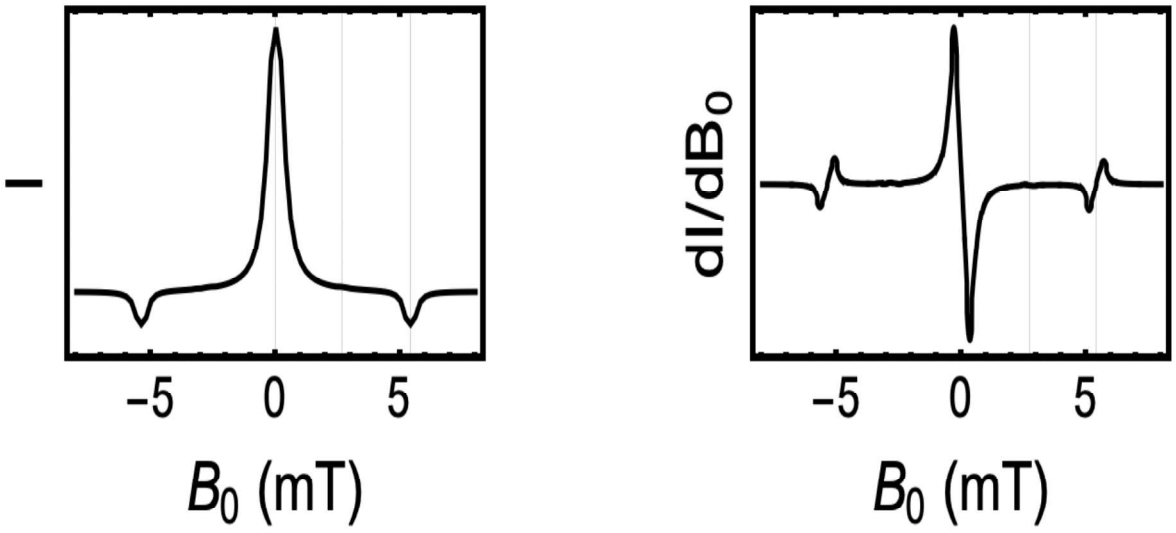

Figure 17. Left: Modeled NZFMR and EDMR trace (corresponds to integrated experimental trace). Right: derivative of left panel. Note the close correspondence between the theoretical results on the right and the experimental results of figure 14.

As mentioned, these simulations are based upon a dipolar interaction term of 0.3mT. The experimental result obtained from the half field measurements is also 0.3mT. The overall close correspondence between the experimental and theoretical NZFMR and EDMR line shapes is also excellent. The very close correspondence between the stochastic Liouville based calculations of Harmon et al and the experimental results is a very strong indication that the overall approach is appropriate. This work demonstrates that, at least for the Si/ SiO_2 system, the NZFMR approach is an analytical tool with the power to provide atomic scale information about electrically active defects. In the case described here, we are identifying Silicon/silicon dioxide interface defects and near interface oxide hole traps. It is well established that these are the most important radiation damage defects in conventional MOS technology.

G. Silicon Carbide and Si Vacancies with Magnetic Nitrogen Nuclei Nearby in SiC MOSFETs: Experiment and Theory

Again, addressing both new systems and defects and the presence of magnetic nuclei, we have made preliminary measurements using NZFMR charge pumping on 4H SiC MOSFETs in which some devices have a very high density of nitrogen atoms close to Si vacancy sites. The device geometries, doping densities etc. are the same in both sets of devices, the only difference is the very high nitrogen density in the close proximity of the silicon vacancies in the NO processed devices.

In figure 18 we show both the raw, lock-in amplifier derived data and integrated near zero field response near zero field (NZF) charge pumping results [5]. Here we compare the response of devices in which a very high concentration of nitrogen is present around the defects (NO annealed) and a second set of samples in which the nitrogen is essentially absent (as grown). Based upon rough experimental and theoretical estimates of the hyperfine interactions, we expect a hyperfine interaction of about 0.2mT. A simulated NZF spectrum based on the 0.2mT hyperfine interactions[5] obtained from the other work is shown in figure 19. There is a rough but reasonable correspondence between the simulation and the experimental results. The theoretical and experimentally determined estimates of the hyperfine parameters is very crude. (Among other things, the hyperfine interactions are not likely to be precisely isotropic.) The complexity of the high spin silicon vacancy also complicates the calculation of the NZFMR response. In spite of all of these problems, the correspondence between the stochastic Liouville based simulation and the experimental results is fairly good.

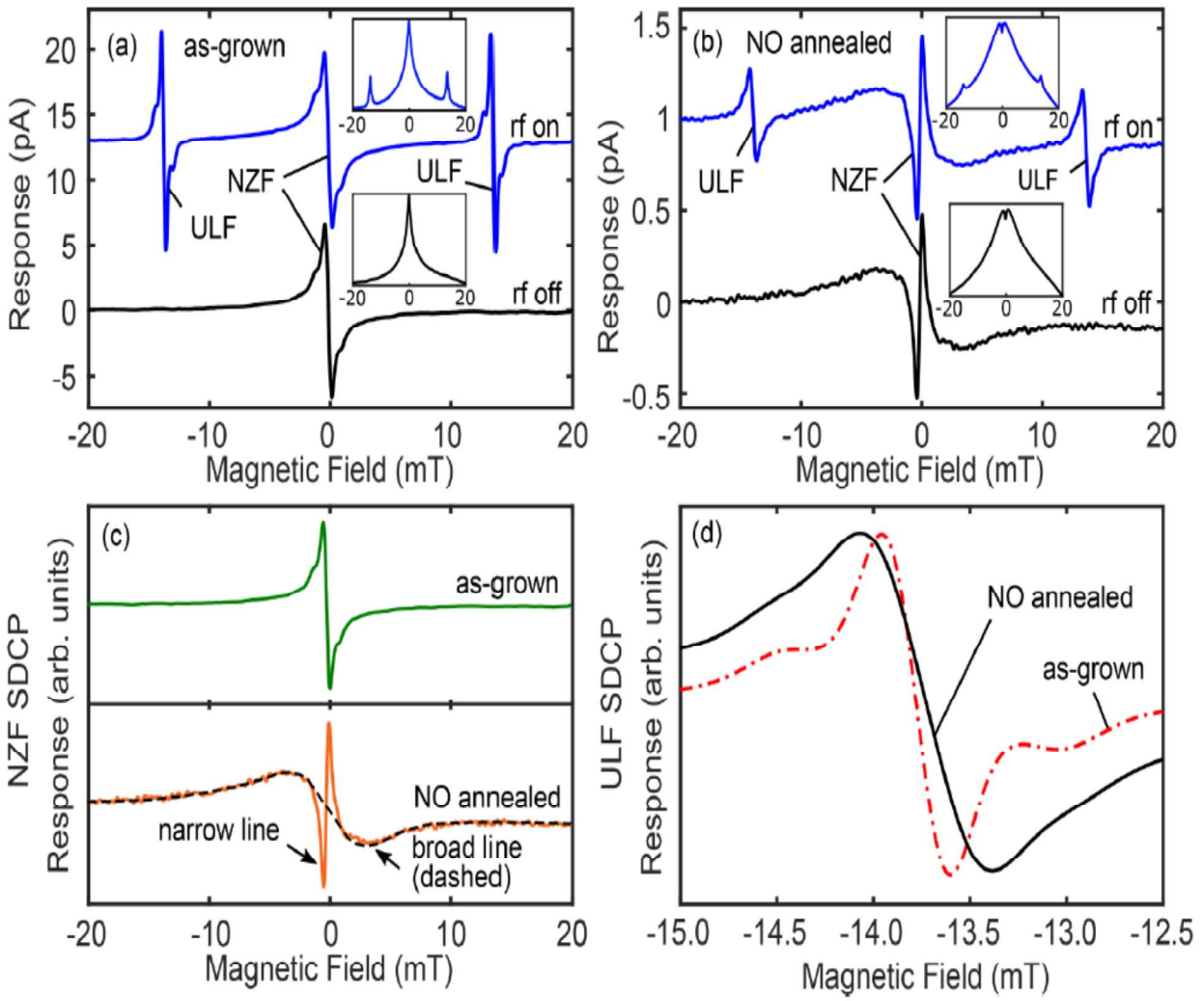

Fig. 18 a) Representative ULF SDCP and NZF SDCP measurements on the as grown and (b) NO annealed samples with and without RF radiation. (c) Is a comparison of the NZF responses from both samples. The dotted black line highlights the "broad" line. The "narrow" line is at the center. (d) Is a comparison of the ULF SDCP spectra from both samples. In all figures, the SDCP amplitudes are normalized to 1 for better comparison. The resonance frequency of the RF coil is 386 MHz and 383 MHz for as grown and NO annealed measurements, respectively. The inset in (a) and (b) are the integrals of the ULF and NZF SDCP responses. For this measurement, V_H = 16 V, V_L = -16 V, and f_{CP} = 1 MHz. Modulation frequency and amplitude are 1 kHz and 0.15 mT, respectively. [5]

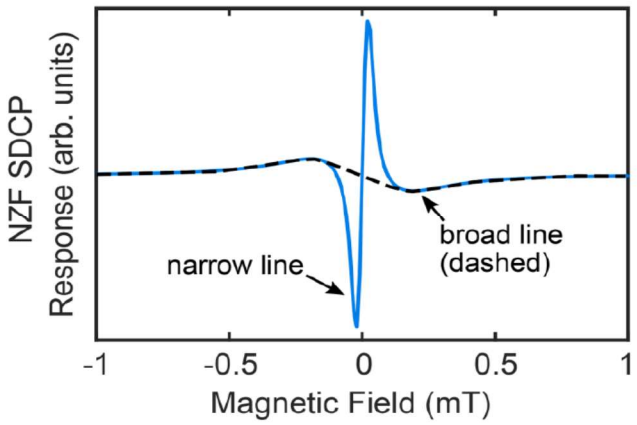

Figure 19: Calculation of NZF SDCP displaying the presence of both the broad and narrow features as observed in the experiments [5]. The inclusion of multiple spins by using a semiclassical approximation for the hyperfine interaction can further broaden the already broad line shape feature. Parameters: a = 0.2 mT, k_S = 0.001 ns^{-1}, k_T = 0.001 ns^{-1}, and f_{CP} = 0.5 MHz.

SiC is known to host several paramagnetic defects of which at least two present a challenge to the existing formalism developed. The stochastic Liouville equations employed thus far have assumed a defect spins state that alternates between 0 and ½ depending upon its occupation. While NZFMR and EDMR have been observed in SiC, our framework, as currently expressed, is not adequate to analyze the neutral divacancy defect (S = 1) and the negatively charged silicon monovacancy (S = 3/2). We elected to study the monovacancy since it is believed to be the relevant in several experiments which strongly indicate that these defects play important roles in the operation of 4H SiC MOSFETs.

With a mind toward recombination, we devised a model where the defect alternates between S= 3/2 (when negatively charged) and S = 1 (when neutral) as an electron is captured by the deep level defect and recombined with a hole. The precursor states to a capture are then S = ½ and S = 1. These two states evolve in their local environment and then combine only if their total spin is S = 3/2. Again the stochastic Liouville equations work well to describe this process.

The complexity of the defect (for example zero field splitting) allows for a wider variety of possible behavior. Fig. 20 is a NZFMR trace when there no zero-field splitting [14].

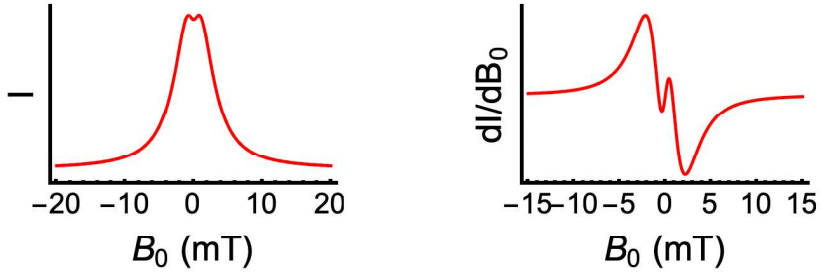

Figure 20. Left: Modeled NZFMR trace for a S = 3/2 spin center. Right: derivative of left panel. Zero field splitting is set to zero. Ref. 14.

Fig. 21 is a NZFMR trace when there is a finite zero field splitting [14]. Distinct resonances form at field values near the value of zero field splitting (chosen to be 4 mT here).

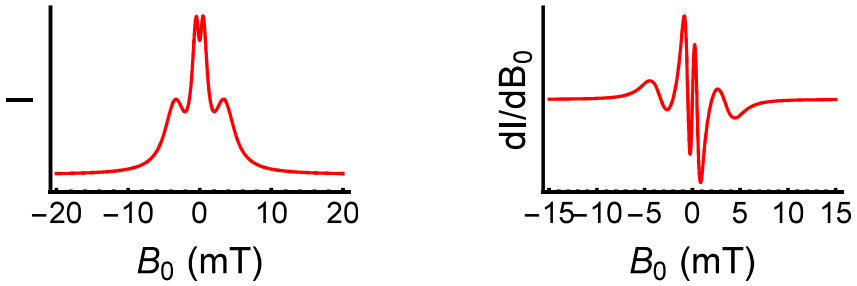

Figure 21. Left: Modeled NZFMR trace for a S = 3/2 spin center. Right: derivative of left panel. Zero field splitting is non-zero. From Ref. 14.

H. NZFMR as a diagnostic for Silicon Nitrides

A material of potential interest is silicon nitride. We have conducted a NZFMR study of silicon nitride films which involves the measurement of the EDMR and NZFMR response of films with seven different stoichiometries. The films are all roughly 50 nm thick. The a-SiN:H thin films differ in composition but the only process parameter that was modified between films was the flow rate of NH_3 to vary the stoichiometry. The measured thickness and N/Si concentration for each film is given in table 1. The leakage current test structure consisted of a Ti/a-SiN:H/p-Si metal-insulator-semiconductor capacitor The leakage current test structure consisted of a Ti/a-SiN:H/p-Si metal-insulator-semiconductor capacitor mounted to a test board and wire bonded. EDMR measurements were made at high fields (v~9.5GHz) and low fields (v~350MHz) to compare the effects of broadening due to spin-orbit coupling and electron-nuclear hyperfine interactions. All measurements were taken at 5 G magnetic field modulation at 1900 Hz with a time constant of 0.3 s. Representative NZFMR and EDMR results are shown in figures 6 and 7. A tabulation of key parameters is presented in Table 1.

Sample	Thickness (nm)	Flow rate NH_3 (sccm)	N/Si Ratio	NZFMR LW (G)	LF LW (G)	X Band LW (G)	Measured g-value
A	46.1	1500	0.432	17.4	9.4	9.6	2.0054
B	45.5	3000	0.677	32.7	9.8	10.1	2.0055
C	46.5	6000	0.866	34.7	11.3	12.4	2.0053
D	48.4	9000	1.026	38.0	12.5	14.3	2.0048
E	51.3	15000	1.052	38.2	13.9	15.0	2.0036
F	50.1	12000	1.182	37.1	13.1	14.4	2.0046
G	52.2	18000	1.268	40.0	14.9	16.3	2.0042

Table 1 Silicon Nitride film parameters.

In Figure 22, the NZFMR response as a function of nitrogen concentration is presented [2]. The lowest concentration of nitrogen resulted in a linewidth (LW) of 17.4 G. The measured NZFMR linewidth increases with increasing nitrogen concentration up to a linewidth of 40.0 G.

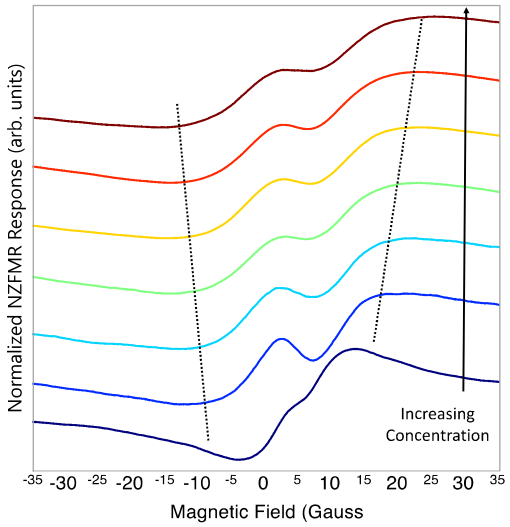

Fig. 22: NZFMR response of the various silicon nitride films is illustrated. The lowest nitrogen concentration results in a linewidth of 9.4 G, increasing up to a linewidth of 14.9 G for the highest nitrogen concentration. (The seven samples of Table 1 are utilized for these measurements.) Ref. 2.

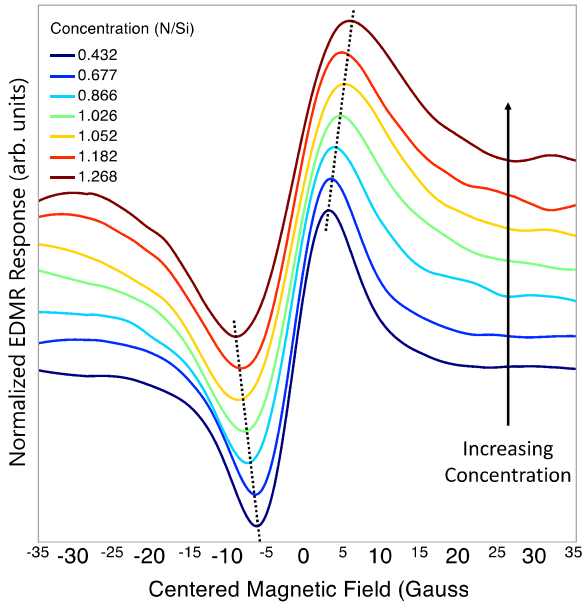

Figure 23: EDMR responses at low field. Ref. 2.

In figure 23, the EDMR response at high field/frequency is shown [2]. The linewidth increases from 9.6 G up to 16.3 G with increasing nitrogen concentration. The measured linewidth for each method is compiled in table 1. The measured linewidth for both the EDMR and the NZFMR measurements follow the same general trend: increasing linewidth with increasing N/Si concentration.

An evaluation of the EDMR data will allow us to extract hyperfine parameters and, with the varying stoichiometries present in these samples, we will be able to apply (and likely refine) the Liouville equation approaches for defect identification during the coming months of the program.

I. NZFMR Studies of Aluminum Oxides for RRAM Devices

We made spin dependent trap assisted tunneling NZFMR measurements on Al_2O_3 oxides on Si, with a thin interlayer of SiO_2. The device structures were provided by a leading industrial research and development laboratory. A representative NZFMR trace is illustrated in figure 24. The NZFMR trace was taken on a 4nm thick Al2O3 film deposited on (100) silicon surface with an aluminum gate. A 2volt positive potential was applied to the gate with the silicon substrate grounded during the measurement. The NZFMR trace is quite broad, extending over 200mT. The great breadth is almost certainly due to the presence of 100% naturally abundant spin 5/2 aluminum nuclei.

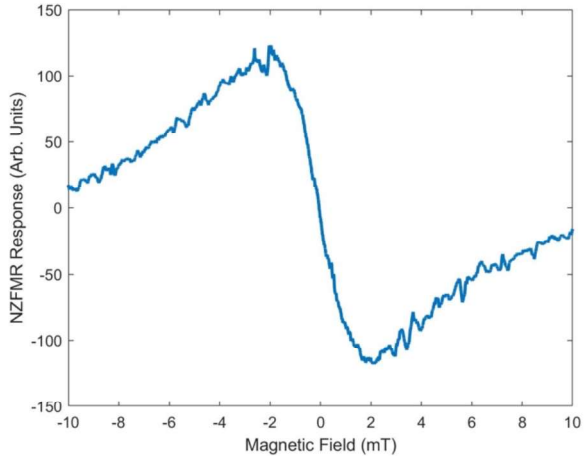

Figure 24: A representative NZFMR trace taken on an MOS capacitor with aluminum oxide thin film 4nm thick with a positive potential of 2 volts applied to the Al gate and the silicon substrate grounded.

J. Demonstration of NZFMR effectiveness when EDMR is screened

We have now shown that one can observe NZFMR spectra in packaged integrated CMOS circuits. These results are shown for commercially available Toshiba NAND2 logic gates operating in the near-OFF regime. Low- and high-frequency EDMR were performed on these integrated circuits, but due to the packaging, no EDMR spectra could be resolved. This directly showcases NZFMR's potential as a non-intrusive method for analyzing quiescent (defect-driven) recombination current in modern integrated circuits.

We used a Toshiba TC7SH00F NAND gate to demonstrate the effect of biasing conditions on the response. For biasing the sample, we used a Stanford Research Systems Preamplifier, Model SR570. For magnetic field manipulation we used a Kepco BOP 100-4M bipolar operational power supply. As shown in figure FIGURE, power supply changes the quasi- static magnetic field, sweeping from -200G to 200G. The preamplifier is used to bias the sample and relay changes in current to the DAQ. The mod box is used in conjunction with the DAQ to control the mod coils.

These are the first recorded observation of NZFMR responses in packaged and commercially available CMOS integrated circuits. This study shows a proof of concept that NZFMR is indeed

useful for studying paramagnetic defects in previously inaccessible scenarios. We observe a significant change in both the amplitude and linewidth of these signals with bias, as is expected from previous NZFMR measurements in custom made test structures. For this study, we biased the NAND gate at intervals of 0.1V from -0.3V to 0.4V. We obtained signals at each of these biases and were able to recognize obvious trends. As bias becomes more positive, the linewidth increases as shown in Fig. 25. It eventually saturates toward the most positive end of our bias study. We also note a general trend of increasing amplitude of NZFMR signal as bias becomes more positive.

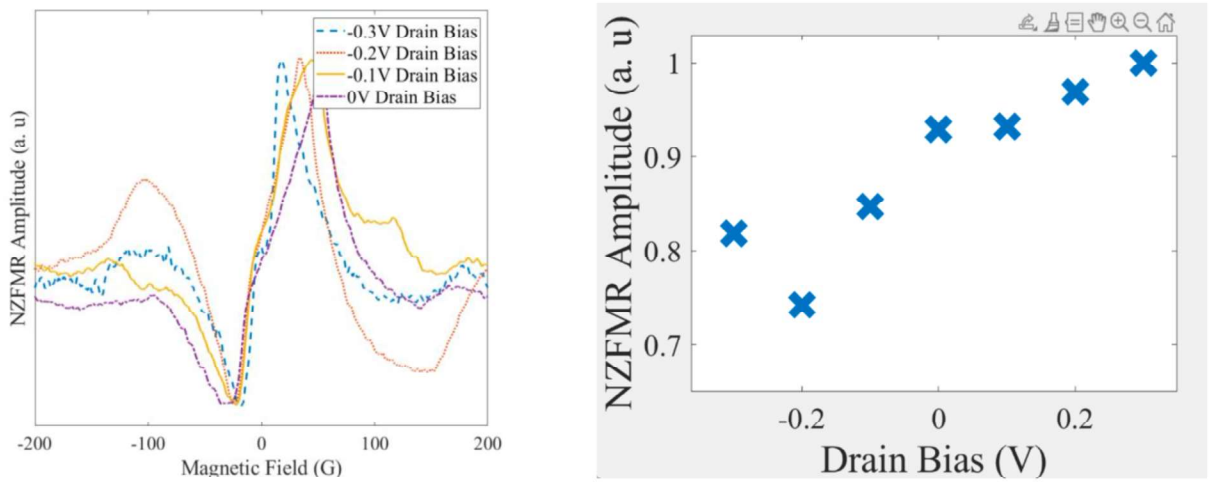

Fig. 25: NZFMR responses in commercial packaged CMOS integrated circuits. The linewidth increases with positive bias, and saturates toward the most positive end of the bias study (left). Also shown is the trend of increasing amplitude of signal as bias becomes more positive (right).

K. Summary

This project was intended to explore near-zero-field magnetoresistive (NZFMR) effects that did not require RF fields in a variety of modern semiconductor devices with insulating barriers of many types. The goal was to provide a defect-identification tool that provided similar specificity as electron paramagnetic resonance or electrically-detected magnetic resonance but did not require microwave fields, so that the approach could be used for vertically integrated devices that were effectively shielded from microwaves. The focus was initially on well characterized SiO2 interfaces, such as the exceptionally well characterized Si/SiO2 interface. Diagnostics of isotopic purification were also achieved for devices isotopically enriched with zero-spin silicon nuclei. NZFMR diagnostics were also demonstrated in silicon nitrides, silicon carbide devices, and the ability of the approach to identify defect type and density was demonstrated. At the conclusion of the effort the NZFMR effects were demonstrated in commercially packaged CMOS integrated circuits. The conclusion is that this approach is a broadly useful approach for defect identification in radiation-damaged, 3D, vertically integrated devices. High accuracy simulations of the defect dynamics in these damaged structures used stochastic Liouville equations to simulate the spin dynamics and identify the hyperfine character of the neighboring atoms surrounding the defects, thus providing a clear identification of the defect type.

Dependence on bias provides additional constraints and helps identify defect density. Initial steps were taken to provide for a simpler fitting method that could be used for routine measurements, and compared to high accuracy simulations.

L. Publications Supported Under this Grant

1. James P. Ashton, Stephen J. Moxim, Patrick M. Lenahan, Colin G. McKay, Ryan J. Waskiewicz, Kennth J. Myers, Michael E Flatte, Nicholas J. Harmon, and Chadwin D. Young, "A New Analytical Tool for the Study of Radiation Efffects in 3-D Integrated Circuits: Near-Zero Field Magnetoresitance Spectroscopy", IEEE Transactions on Nuclear Science 66, 428 (2019). https://doi.org/10.1109/TNS.2018.2885300
2. Ryan J. Waskiewicz, Elias B. Frantz, Patrick M. Lenahan, Sean W. King, Nicholas J. Harmon, and Michael E. Flatte, "Identifying Defects Responsible for Leakage Currents in Thin Dielectric Films", IEEE IIRW Final Report (Conference Proceedings) page 48, (2018). Edited by Zakariae Chbili, Stanislav Tyaginov https://doi.org/10.1109/IIRW.2018.8727077
3. Stephen J. Moxim , James P. Ashton, Patrick M. Lenahan, Michael E. Flatté , Nicholas J. Harmon , and Sean W. King, "Observation of Radiation-Induced Leakage Current Defects in MOS Oxides With Multifrequency Electrically Detected Magnetic Resonance and Near-Zero-Field Magnetoresistance", IEEE Transactions on Nuclear Science 67, 228 (2020). https://doi.org/10.1109/TNS.2019.2958351
4. Nicholas J. Harmon , Stephen R. McMillan, James P. Ashton, Patrick M. Lenahan, and Michael E. Flatté, "Modeling of Near Zero-Field Magnetoresistance and Electrically Detected Magnetic Resonance in Irradiated Si/SiO2 MOSFETs", IEEE Transactions on Nuclear Science 67, 1669 (2020). https://doi.org/10.1109/TNS.2020.2981495
5. M. A. Anders, P. M. Lenahan, N. J. Harmon and M. E. Flatté, "A technique to measure spin-dependent trapping events at the metal-oxide-semiconductor field-effect transistor interface: Near zero field spin-dependent charge pumping", J. Appl. Phys. 128, 244501 (2020). https://doi.org/10.1063/5.0027214
6. Elias B. Frantz, Nicholas J. Harmon, Stephen R. McMillan, Stephen J. Moxim, Michael E. Flatté, Patrick M. Lenahan, "Extraction of Isotropic Electron-Nuclear Hyperfine Coupling Constants of Paramagnetic Point Defects from Near-Zero Field Magnetoresistance Spectra via Least Squares Fitting to Models Developed from the Stochastic Quantum Liouville Equation", Journal of Applied Physics 128, 124504 (2020). https://doi.org/10.1063/5.0019875
7. M.A. Anders, P.M. Lenahan, and J.T. Ryan, "Wafer level near zero field spin dependent charge pumping effects of nitrogenon 4H SiC MOSFETs", Materials Science Forum 1004, 573 (2020). https://doi.org/10.4028/www.scientific.net/MSF.1004.573

8. E.B. Frantz, D. J. Michalak, N. J. Harmon, E. M. Henry, S. J. Moxim, M. E. Flatte, S. W. King, J. S. Clarke, and P. M. Lenahan, "Electrically detected magnetic resonance and near-zero field magnetoresistance in $^{28}Si/^{28}SiO_2$," J. Appl. Phys. vol. 130, art no. 065701(2021): https://doi.org/10.1063/5.0057871
9. E.B. Frantz, D. J. Michalak, N. J. Harmon, E. M. Henry, S. J. Moxim, M. E. Flatte, S. W. King, J. S. Clarke, and P. M. Lenahan, "Effects of ^{29}Si and ^{1}H on the near-zero field magnetoresistance response of Si/SiO_2 interface states: Implication for oxide tunneling currents," Appl. Phys. Lett. vol. 119, art no.184101 (2021). https://doi.org/10.1063/5.0066640
10. E.B. Frantz, D. J. Michalak, N. J. Harmon, E. M. Henry, S. J. Moxim, M. E. Flatte, S. W. King, J. S. Clarke, and P. M. Lenahan, "Extraction of dipolar coupling constants from low-frequency electrically detected magnetic resonance and near-zero field magnetoresistance spectra via least squares fitting to models developed from the stochastic quantum Liouville equation," J. Appl. Phys. 130, art no. 234401 (2021): https://doi.org/10.1063/5.0075460.
11. F. V. Sharov, S. J. Moxim, D. R. Hughart, G. S. Haase, C. G. McKay, P. M. Lenahan, "Probing the Atomic Scale Mechanisms of Time Dependent Dielectric Breakdown in Si/SiO_2 MOSFETs," IEEE Trans. Device Mater. Reliab. (2022) (Early Access) (Invited): https://doi.org/10.1109/TDMR.2022.3186232.
12. S. J. Moxim, F. V. Sharov, D. R. Hughart, G. S. Haase, C. G. McKay, P. M. Lenahan, "Atomic-scale defects generated in the early/intermediate stages of dielectric breakdown in Si/SiO_2 transistors," Appl. Phys. Lett. vol. 120, art. no. 063502 (2022): https://doi.org/10.1063/5.0077946.
13. S. J. Moxim, F. V. Sharov, D. R. Hughart, G. S. Haase, C. G. McKay, E. B. Frantz, P. M. Lenahan, "Near-Zero-Field Magnetoresistance Measurements: A Simple Method to Track Atomic-Scale Defects involved in Metal-Oxide-Semiconductor Device Reliability," Rev. Sci. Instrum. (2022) (In Review).
14. N. J. Harmon, J. P. Ashton, P. M. Lenahan and M. E. Flatté, "Near-Zero-Field Spin-Dependent Recombination Current and Electrically Detected Magnetic Resonance from the Si/SiO2 interface", APL Materials (2022) (in review).
15. K. J Meyers, Ph. D. Thesis, (2022).
16. S. J. Moxim, Ph. D. Thesis, (2022).
17. E. B. Frantz, Ph. D. Thesis, (2022).
18. M. Elko, SISC 2022 Abstract Submission (In Preparation) (2022).